Journal of Molecular Graphics and Modelling 51 (2014) 158–167

Contents lists available at ScienceDirect

Journal of Molecular Graphics and Modelling

journal homepage: www.elsevier.com/locate/JMGM

Molecular dynamics study on conformational differences between dGMP and 8-oxo-dGMP: Effects of metal ions

Shin-ichi Fujiwara*, Kenichiro Sawada, Takashi Amisaki

Department of Biological Regulation, Faculty of Medicine, Tottori University, 86 Nishi-cho, Yonago 683-8503, Japan

ARTICLE INFO

Article history:
Accepted 22 May 2014
Available online 2 June 2014

Keywords:
Mononucleotide
Molecular dynamics simulations
8-oxo-dGTP
Divalent ion
Nucleotide-sanitizing enzyme
Conformation

ABSTRACT

The modified nucleotide base 7,8-dihydro-8-oxo-guanine (8-oxo-G) is one of the major sources of spontaneous mutagenesis. Nucleotide-sanitizing enzymes, such as the MutT homolog-1 (MTH1) and nudix-type motif 5 (NUDT5), selectively remove 8-oxo-G from the cellular pool of nucleotides. Previous studies showed that, although the *syn* conformation generally predominates in purine nucleotides with a bulky substituent at the 8-position, 8-oxo-dGMP binds to both MTH1 and NUDT5 in the *anti* conformation. This study was initiated to investigate the possibility that 8-oxo-dGMP itself may adopt the *anti* conformation. Molecular dynamics simulations of mononucleotides (dGMP, 8-oxo-dGMP) in aqueous solution were performed. 8-oxo-dGMP adopted the *anti* conformation as well as the *syn* conformation, and the proportion of adopting the *anti* conformation increased in the presence of metal ions. When 8-oxo-dGMP was in the *anti* conformation, a metal ion was located between the oxygen atom of phosphate and the oxygen atom at the 8-position of 8-oxo-G. The types of stable *anti* conformations of 8-oxo-dGMP differed, depending on the ionic radii and charges of coexisting ions. These data suggested a role for metal ions, other than as cofactors for the hydrolysis of the di- and tri-phosphate forms of mononucleotides; that the metal ions help retain the *anti* conformation of the N-glycosidic torsion angle of 8-oxo-dGMP to promote the binding between the 8-oxo-G deoxynucleotide and the nucleotide-sanitizing enzymes.

1. Introduction

Nucleic acid bases in cells are easily modified by reactive oxygen species. Among these modified bases, 7,8-dihydro-8-oxo-guanine (8-oxo-G) is a major source of spontaneous mutagenesis. Cells have evolved different mechanisms to reduce the mutagenic effect of 8-oxo-G [1]. One mechanism is nucleotide-sanitization. This involves selective removal of modified bases from the nucleotide pool by nucleotide hydrolases so that the modified nucleotides cannot be incorporated into DNA by DNA polymerases. For example, 8-oxo-dGTPases such as MutT and the MutT homolog-1 (MTH1) hydrolyze 8-oxo-dGTP into 8-oxo-dGMP [1,2]. 8-oxo-dGDPases such as nudix (nucleoside diphosphate linked moiety X)-type motif 5 (NUDT5) hydrolyze 8-oxo-dGDP into 8-oxo-dGMP [3]. The enzymes MutT, MTH1, and NUDT5 can discriminate among the slight structural differences between normal and modified nucleotides.

Structural studies have been performed to investigate the specific recognition of 8-oxo-G by MutT [4], MTH1 [5], and NUDT5 [6]. Crystal structures indicated that 8-oxo-dGMP bound to MutT adopted the *syn* conformation about the N-glycosidic bond that links the base to the sugar. Hydrogen bonds were observed between the enzyme and the oxygen atom at the 8-position (O8 atom) of 8-oxo-dGMP [4]. On the other hand, 8-oxo-dGMP was bound to MTH1 and NUDT5 in the *anti* and the *high-anti* conformations, respectively [5,6]. However, the *syn* conformation should generally predominate in purine nucleotides with a bulky substituent at the 8-position [7]. No direct interaction, such as hydrogen bonding between MTH1 and NUDT5 and the O8 atom of 8-oxo-dGMP, was observed in the crystal structures of either enzyme [5,6].

Conformations of mononucleotides have been analyzed experimentally [7], and recently, by computational analyses. Quantum mechanics (QM) calculations have been widely performed to compare potential energies of the *anti* and *syn* conformations of mononucleotides [8–18]. Although these QM results gave insights into preferable conformations of mononucleotides in terms of the potential energies, water molecules and ions were either excluded or included only implicitly in many of these studies. The N-glycosidic conformation of 8-oxo-dGMP can be affected by water molecules and ions. However, it is generally very difficult to perform QM calculations that include water molecules or ions explicitly. On the other hand, although molecular dynamics (MD) simulations are less rigorous, they can generate a collection of

* Corresponding author. Tel.: +81 858 38 6356; fax: +81 859 38 6350.
E-mail address: fujiwara@med.tottori-u.ac.jp (S.-i. Fujiwara).

http://dx.doi.org/10.1016/j.jmgm.2014.05.007
1093-3263/

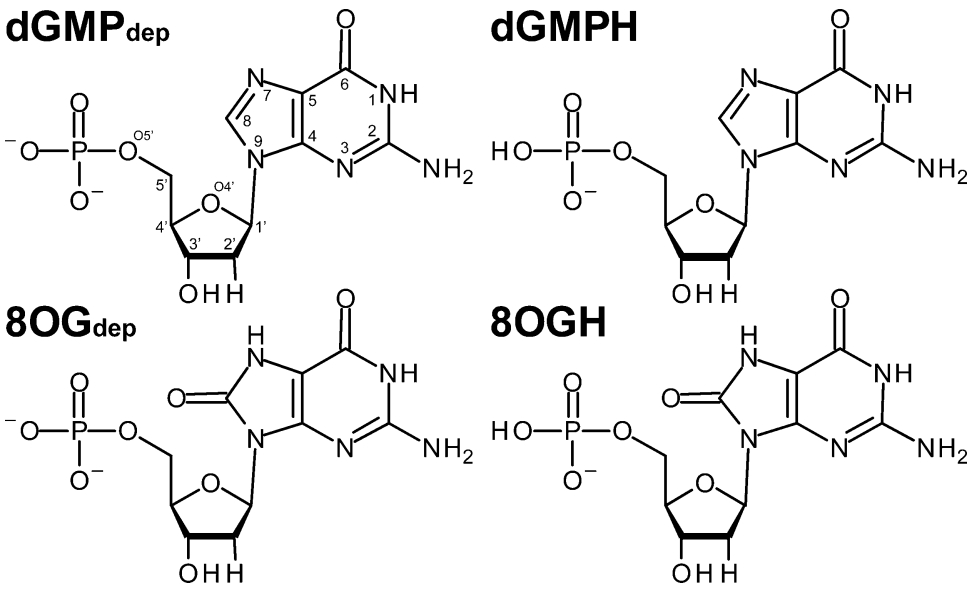

Fig. 1. Mononucleotide models analyzed in this study. Atom numbering is shown for $dGMP_{dep}$.

conformations of a small ligand in explicit water molecules and ions [19]. The preferable conformation of mononucleotides can be found by comparing the numbers of the *anti* or *syn* conformations obtained by MD simulations. Numerous MD simulations of mononucleotides complexed with G protein-coupled receptors [20], and gas-phase conformations of mononucleotides [8], have been reported. However, to our knowledge, no previously published works apply MD simulations to 8-oxo-G mononucleotides in explicit solvents.

In this study, we performed MD simulations of dGMP and 8-oxo-dGMP in explicit solvents. Under the assumption that the proportion of the *anti* or *syn* conformations of mononucleotides might be influenced by water molecules, metal ions, or the state of protonation of the phosphate groups of mononucleotides, we examined different protonation states of phosphate, and the effects of different kinds of metal ions in MD simulations. We also tested different starting structures and two different parameters related to the N-glycosidic torsion angle. A series of simulations indicated that 8-oxo-dGMP can adopt the *anti* conformation, and that exposure to metal ions increases the proportion of adopting the *anti* conformation.

2. Methods

2.1. Model construction

The four kinds of mononucleotides studied were phosphate-deprotonated dGMP ($dGMP_{dep}$), phosphate-protonated dGMP (dGMPH), phosphate-deprotonated 8-oxo-dGMP ($8OG_{dep}$), and phosphate-protonated 8-oxo-dGMP (8OGH) (Fig. 1). Given that the phosphate group of nucleotides has p*Ka* = 5.9–7.0 [21], both deprotonated ($dGMP_{dep}$, $8OG_{dep}$) and protonated (dGMPH, 8OGH) forms of mononucleotides were considered. A series of model constructions and MD simulations were performed using AMBER11 and AmberTools1.5 [22]. The force field parameters of mononucleotides were generated by the antechamber module, based on the ff99SB force field [23]. Two parameters were examined for the dihedral angle of the N-glycosidic bond. One was the standard parameter generated by the antechamber module (denoted by χ_{std}). The other was the modified parameter (denoted by χ_{mod}), which was based on the literature [24]. The force field parameters of 8-oxo-G [25] and protonated phosphate [26] were based on published values. QM calculations of the mononucleotides with the *anti* conformation were performed at the HF/6-31G**//B3LYP/cc-pVTZ level of theory in implicit diethylether (energy minimization) and water (point-charge calculation) using Gaussian 03 [27]. Restrained electrostatic potential was used as the charge method. Both the *anti* and *syn* conformations were used as the initial structures to examine the effects on the MD simulations. The *syn* conformation of each mononucleotide was created by rotating the N-glycosidic bond manually from the energy-minimized *anti* conformation using Discovery Studio Visualizer (version 3.5). The force field parameters used in this study are summarized in Doc. S1 of Supporting information.

The LEaP module was used to construct a model of each mononucleotide in explicit solvents. A truncated octahedral box of TIP3P water [28] was added around the *anti* or *syn* conformation of each mononucleotide, with the buffering distance set to at least 15 Å. An ion was placed at the 1.0-Å grid point of the lowest electrostatic potential energy around each starting conformation (Fig. S1). Either no ion, one divalent (Mg^{2+}), or two monovalent (Na^+) ions were placed in the phosphate-deprotonated systems ($dGMP_{dep}$ and $8OG_{dep}$). Either no ion or one ion (Mg^{2+} or Na^+) was placed in the phosphate-protonated systems (dGMPH and 8OGH). In addition, one Ca^{2+} ion or two Li^+ ions were placed in the $8OG_{dep}$ system, and one ion (Ca^{2+} or Li^+) was placed in the 8OGH system. Positions of the metal ions placed for each starting conformation are shown in Fig. S1. The force field parameters of the ions were taken from the literature [29]. The total number of mononucleotide, water molecules, and ions was set to 2130 in all the systems. In summary, 12 systems for $dGMP_{dep}$ and dGMPH, and 16 systems for $8OG_{dep}$ and 8OGH were constructed, differing in the N-glycosidic bond parameters (χ_{std} or χ_{mod}), ions (no ion, Na^+, Mg^{2+}, Li^+, Ca^{2+}), and the initial conformation (*anti* or *syn*) of the mononucleotides.

2.2. MD simulations of mononucleotides

The pmemd module was used for energy minimization and MD calculations. We performed 500 steps of energy minimization constraining the mononucleotide and ions, followed by 500 steps of energy minimization with no constraints. For each system, constant-volume MD calculations were carried out for 80 ps, during which the temperature was raised from 10 to 310 K, followed by a total of 200 ps constant-pressure MD calculations for equilibration. Production runs, each lasting 5.2 ns, were conducted for

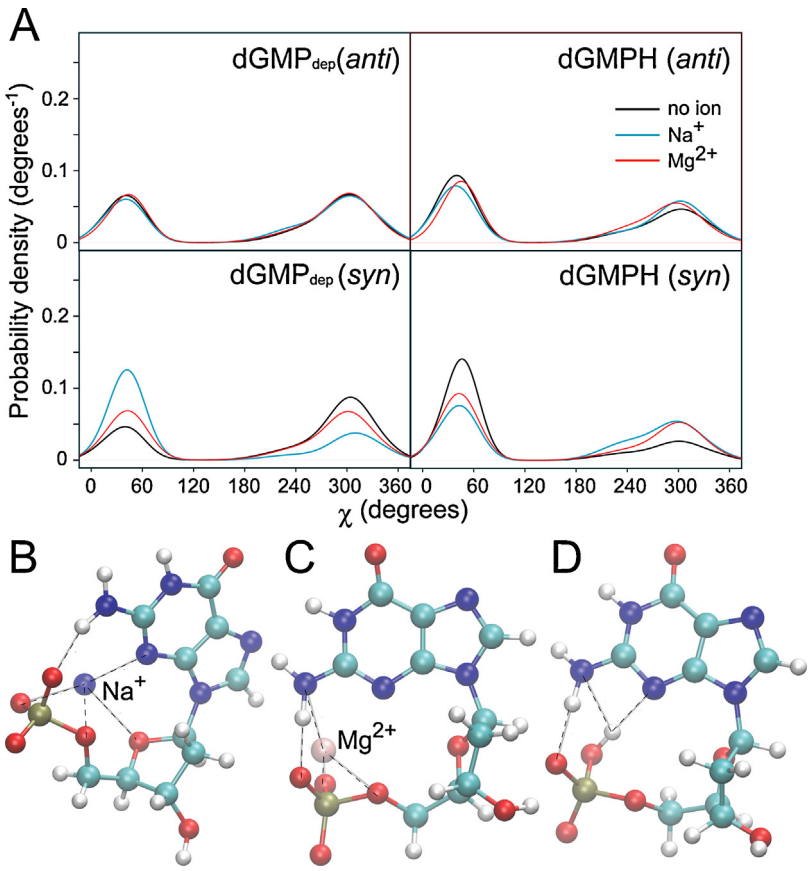

Fig. 2. (A) Probability density of the χ angle of dGMP in the dGMP$_{dep}$ and dGMPH systems using the standard N-glycosidic bond parameter (χ_{std}). Initial structures (*anti*/*syn*) are indicated in parentheses. (B) One of the *syn* conformations observed in the dGMP$_{dep}$ system with Na^+. (C) One of the *syn* conformations observed in the dGMP$_{dep}$ system with Mg^{2+}. (D) One of the *syn* conformations observed in the dGMPH system. These molecular diagrams are generated with VMD (version 1.9.1) [49].

each system. Temperature and pressure were maintained using the weak-coupling algorithm [30] with coupling constants τ_T and τ_P of 1.0 ps and 0.2 ps, respectively (310 K, 1 atm). The non-bonded list was generated using an atom-based cutoff of 10 Å. The long-range electrostatic interactions were handled by the particle mesh Ewald algorithm [31]. In non-neutralized systems (no-ion systems, and dGMPH and 8OGH systems with divalent ions), a uniform neutralizing plasma was used to prevent the energy in the net-charge system from diverging [32]. The time step was set to 2.0 fs, and the SHAKE algorithm [33] was used. For each system, MD simulations were performed twice by changing the initial velocity of each atom, which was assigned from a Maxwell-Boltzmann distribution at 10 K. Snapshots were saved every 1 ps. For analyses, 20,000 snapshots, each between 201 ps and 5.2 ns, were used. Published values were used for torsion angles of the sugar-phosphate backbone (β, γ), and the N-glycosidic torsion angle (χ) that determines the *syn*, *anti*, and *high-anti* conformations [34]. The torsion angles χ, β, and γ were defined by O4′–C1′–N9–C4, P–O5′–C5′–C4′, and O5′–C5′–C4′–C3′, respectively.

3. Results and discussion

3.1. Conformation of dGMP in explicit solvent

Fig. 2A shows the probability density of the χ angle (N-glycosidic torsion angle) of dGMP with a standard N-glycosidic torsion parameter (χ_{std}). In both dGMP$_{dep}$ and dGMPH systems, dGMP adopted the *syn* (0–90°, 330–360°), *anti* (90–270°) and *high-anti* (270–330°) conformations. It is generally recognized that steric constraints restrict bases in purine nucleotides to two stable conformations (*anti* and *syn*) with respect to deoxyribose [35]. Given that QM conformational studies involving implicit water with a Na^+ counterion [17] indicated that the potential energy of dGMPH was lower in the *syn* conformation than in the *anti* conformation by only 1.5 kJ/mol, it is reasonable to consider that dGMPH can adopt both conformations in water. Accordingly, the MD simulation of dGMPH also indicated that dGMPH, in the presence of Na^+, adopted a conformational ratio of about 54 (*anti* and *high-anti*): 46 (*syn*).

In the dGMP$_{dep}$ systems, when the *syn* conformation was the initial structure, the proportion of the *syn* conformation was larger in the presence than in the absence of metal ions (Fig. 2A). This resulted from the longer maximum lifetime, which is defined as the time from the moment of the original *syn*/*anti* conformation until the moment at which it is changed into the opposite *anti*/*syn* conformation (Table 1). In examining a series of the *syn* conformations with the maximum lifetime, characteristic *syn* conformations of dGMP were observed in the presence of metal ions (Fig. 2B and C). In dGMP that adopted the *syn* conformation, a hydrogen bond was formed between the hydrogen atom of the guanine 2-amino group and the oxygen atom of phosphate. This interaction probably resulted from a longer maximum lifetime in the *syn* conformation than in the *anti* conformation (Table 1). Furthermore, in the *syn* conformation of dGMP, electrostatically favorable interactions were formed between Na^+ or Mg^{2+} and the nitrogen and oxygen atoms of dGMP (Fig. 2B and C).

In the dGMPH system without ions, the proportion of the *syn* conformation was larger than that in the dGMP$_{dep}$ system (Fig. 2A), owing to a longer maximum lifetime of the *syn* conformation in the dGMPH system than in the dGMP$_{dep}$ system (Table 1). In the *syn* conformation with maximum lifetime, a hydrogen bond was

Table 1
Frequency of the *anti*-to-*syn* and *syn*-to-*anti* transitions, and maximum lifetime of the *anti*/*syn* conformations in MD simulations of dGMP using the χ_{std} parameter.

Model	Initial structure	Frequency of transitions	Maximum lifetime (ps)[a]	
			Syn	*Anti*
$dGMP_{dep}$	*anti*	680	462	196
	syn	801	329	206
$dGMP_{dep} + Na^+$	*anti*	674	424	246
	syn	484	3529	101
$dGMP_{dep} + Mg^{2+}$	*anti*	595	1016	212
	syn	577	579	188
dGMPH	*anti*	488	668	262
	syn	255	1490	175
$dGMPH + Na^+$	*anti*	544	455	221
	syn	444	672	329
$dGMPH + Mg^{2+}$	*anti*	440	1060	425
	syn	433	1159	359

[a] The *syn* and *anti* conformations are defined as χ angle of 0–90° and 330–360°, and 90–330°, respectively. The *high-anti* conformations are included in the *anti* conformation.

formed between the nitrogen atoms of guanine and the phosphate hydrogen atom (Fig. 2D). These interactions should also occur in the $8OG_{dep}$ and 8OGH systems, because the only differences between dGMP and 8-oxo-dGMP are the kind of atoms found at the 8-position of guanine, and the protonation of the nitrogen atom at the 7-position of guanine (Fig. 1).

3.2. Conformation of 8-oxo-dGMP in explicit solvent

Fig. 3A shows the probability density of the χ angle of 8-oxo-dGMP under the χ_{std} parameter. In both $8OG_{dep}$ and 8OGH systems, 8-oxo-dGMP mainly adopted the *syn* conformation. This result was consistent with an earlier experimental analysis [7]. As were the cases with the $dGMP_{dep}$ and dGMPH systems, the maximum lifetime of the *syn* conformation was longer in the $8OG_{dep}$ and 8OGH systems with metal ions than in those systems without ions (Table 2). On the other hand, a large proportion for the *anti* conformation was observed in the $8OG_{dep}$ and 8OGH systems with Mg^{2+} (Fig. 3A). When the *anti* conformation was the initial structure, no *anti*-to-*syn* transition occurred during the MD simulations (Table 2). This suggested that 8-oxo-dGMP retained the *anti* conformation through a strong interaction between 8-oxo-dGMP and Mg^{2+}. In the *anti* conformations observed in the $8OG_{dep}$ and 8OGH systems, Mg^{2+} was, in most cases, located between the oxygen atom of phosphate and the O8 atom (Fig. S2), thus forming electrostatic interactions with the O8 atom and the phosphate oxygen atom of 8-oxo-dGMP to retain the *anti* conformation (Fig. 3B and C). Divalent cations such as Mg^{2+} or Mn^{2+} serve as cofactors of MTH1 [36–38] and NUDT5 [6] and play an important role in the hydrolysis of the di- and tri-phosphate forms of the mononucleotide. These MD results implied another role of Mg^{2+}; Mg^{2+} retains the stable *anti* conformations of 8-oxo-dGMP for the binding of the mononucleotide to the enzymes.

Table 2
Frequency of the *anti*-to-*syn* and *syn*-to-*anti* transitions, and maximum lifetime of the *anti*/*syn* conformations in MD simulations of 8-oxo-dGMP using the χ_{std} parameter.

Model	Initial structure	Frequency of transitions	Maximum lifetime (ps)[a]	
			Syn	*Anti*
$8OG_{dep}$	*anti*	80	816	18
	syn	86	909	89
$8OG_{dep} + Na^+$	*anti*	245	2470	20
	syn	68	1402	10
$8OG_{dep} + Mg^{2+}$	*anti*	0	0	≥5000[b]
	syn	64	1710	11
8OGH	*anti*	104	1286	128
	syn	108	847	160
$8OGH + Na^+$	*anti*	38	1899	32
	syn	36	1939	22
$8OGH + Mg^{2+}$	*anti*	0	0	≥5000[b]
	syn	129	1523	95

[a] See footnotes of Table 1.
[b] The *anti* conformationis retained during 5 ns in both of the MD runs. The stability of the *anti* conformation is discussed in *Conformational sampling of mononucleotide using MD simulations* in Section 3.

The *syn*-to-*anti* transition was also observed in 8-oxo-dGMP, as shown by the frequency of the observed transitions (Table 2). When the *syn* conformation was the initial structure, the maximum lifetime during which 8-oxo-dGMP retained the *anti* conformation was approximately 100 ps. This indicated that the *syn* conformation of 8-oxo-dGMP shifted to the *anti* conformation, and that the *anti* conformation was retained for about 100 ps (Table 2). Examination of the *anti* conformation at the maximum lifetime indicated hydrogen bonding occurred between the O8 atoms and the hydrogen atom of phosphate in the 8OGH system without ions (Fig. 3D). In the $8OG_{dep}$ system with Mg^{2+}, Mg^{2+} formed electrostatic interactions with the O8 atom and the phosphate oxygen atom of 8-oxo-dGMP to retain the *anti* conformation (Fig. 3E). Despite that, the interaction lasted for only 100 ps. This suggested that the *anti* conformations observed as Fig. 3C and E differed from each other.

To examine differences in the *anti* conformations of 8-oxo-dGMP in detail, we analyzed other torsion angles of the mononucleotides, pseudorotation of the deoxyribose ring, and the torsion angles of the sugar-phosphate backbone (β, γ). These angles are associated with the interactions between 8-oxo-dGMP and Mg^{2+}. Although no remarkable difference in the pseudorotation was observed between the no-ion systems and the Mg^{2+} systems (Figs. S3–S10), the distribution pattern of the β and γ angles was quite different between the systems (Fig. 4). The β and γ angles observed in the stable *anti* conformations were within the range of (120–160°/210–250°, 40–100°) and (60–210°, 40–70°) in the $8OG_{dep}$–Mg^{2+} and the 8OGH–Mg^{2+} systems, respectively. However, some of the other *anti* conformations observed through the *syn*-to-*anti* transitions were within the range of the β and γ angles in which stable *anti* conformations were observed. This suggested that 8-oxo-dGMP may shift to the stable *anti* conformation after the *syn*-to-*anti* transition in the presence of Mg^{2+}, although the stable *anti* conformation was not observed after the *syn*-to-*anti* transition in the present MD simulations.

In the crystal structures of MTH1 (PDB: 3ZR0) [5] and NUDT5 (PDB: 3AC9 and PDB: 3L85) [6], the respective β and γ angles of 8-oxo-dGMP and 8-oxo-dGDP were 262.04° and 291.69° (chain A of MTH1), 237.21° and 302.21° (chain B of MTH1), 105.22° and 273.03° (PDB: 3AC9, in the presence of Mn^{2+}), and 140.81° and 211.71° (PDB: 3L85, in the absence of ions). Comparison of these β and γ angles with those obtained from the MD simulations (Fig. 4) indicated that 8-oxo-dGMP does not bind to these enzymes in the *anti* conformation observed through MD simulations.

There are several points to note for the crystal structure of NUDT5 (PDB: 3AC9) concerning the selective recognition of 8-oxo-dGDP that has adopted the *anti* conformation [6]. First, the guanine base is located between two tryptophan side chains. The difference in electron distribution between guanine and 8-oxo-G may result in different strengths of interaction with the tryptophan residues. This is somewhat similar to the recognition of methylated bases by 3-methyladenine glycosylase from *Escherichia coli* [39]. Second,

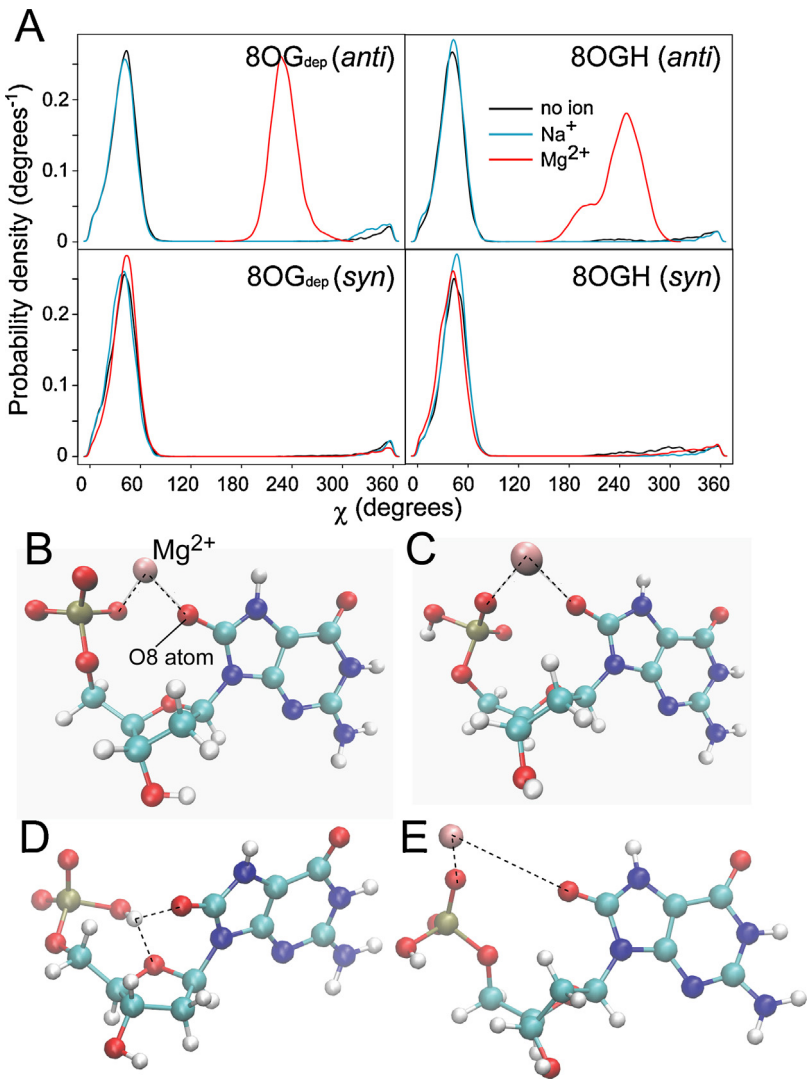

Fig. 3. (A) Probability density of the χ angle of 8-oxo-dGMP in the 8OG$_{dep}$ and 8OGH systems using the χ_{std} parameter. Initial structures (*anti*/*syn*) are indicated in parentheses. (B) One of the *anti* conformations observed in the 8OG$_{dep}$ system with Mg^{2+}. χ, β, and γ angles are 218.6°, 134.9°, and 51.9°, respectively. (C) One of the *anti* conformations observed in the 8OGH system with Mg^{2+}. The angles of χ, β, and γ are 240.3°, 82.3°, and 40.5°, respectively. (D) One of the *anti* conformations observed in the 8OGH system without ions during the *syn*-to-*anti* transition. The angles of χ, β, and γ are 247.2°, 270.1°, and 190.3°, respectively. (E) One of the *anti* conformations observed in the 8OGH system with Mg^{2+} during the *syn*-to-*anti* transition. The angles of χ, β, and γ are 261.7°, 180.5°, and 65.3°, respectively. These molecular diagrams are generated with VMD (version 1.9.1) [49].

a water-mediated hydrogen bond is formed between N7(H) of 8-oxo-G and a carbonyl oxygen of tyrosine. This bond would not be formed between a normal guanine and NUDT5. Third, the *anti* conformation, with a much more extended conformation compared to that observed in the MD simulations, is stabilized by interactions between the phosphate groups of 8-oxo-dGDP and Mn^{2+}. Based on these observations, the selective recognition of NUDT5 and the *anti* conformation of 8-oxo-dGDP can be explained. Some bias for an *anti* conformation in 8-oxo-dGMP mediated by metal ions, which was observed in the MD simulations, may assist in this mechanism. The *anti* conformations observed in the 8OG$_{dep}$ and 8OGH systems may thus play a role in retaining the *anti* conformation until binding of 8-oxo-G mononucleotides to the enzyme occurs.

3.3. Conformational analyses of dGMP and 8-oxo-dGMP using the modified N-glycosidic torsion angle parameter

Recent works have proposed various force field modifications of the χ torsional potential for DNA and RNA based on QM calculations of small molecular models that represent mononucleotides [24,40,41]. In this study, the modified parameter (χ_{mod}) was taken from the literature [24]. This was proven to be suitable for MD simulations of DNA duplexes [24]. The difference between the χ_{std} and χ_{mod} parameters lies in an energy barrier between the *anti* and *syn* conformations of mononucleotides. The energy barrier was higher in the χ_{mod} parameter than in the χ_{std} parameter [24]. Put differently, the *anti*-to-*syn* or *syn*-to-*anti* conformational transition can occur less frequently in MD simulations that use the χ_{mod} parameter than those that use the χ_{std} parameter. In MD simulations of the dGMP$_{dep}$ and dGMPH systems using the χ_{mod} parameter, the frequency of the transition was much less than that of the χ_{std} parameter (Table 3). Together with the higher energy barrier in the χ_{mod} parameter, the maximum lifetime of the *anti* conformation was longer with the χ_{mod} parameter than with the χ_{std} parameter in both mononucleotides (Tables 3 and 4).

Fig. 5 shows the probability density of the χ angle of mononucleotides using the χ_{mod} parameter. In the dGMP$_{dep}$ systems, the proportion of the *anti* conformation was much larger than that of the *syn* conformation, compared with the case of the χ_{std} parameter. In the dGMP$_{dep}$ no-ion system, dGMP adopted mainly the *anti*

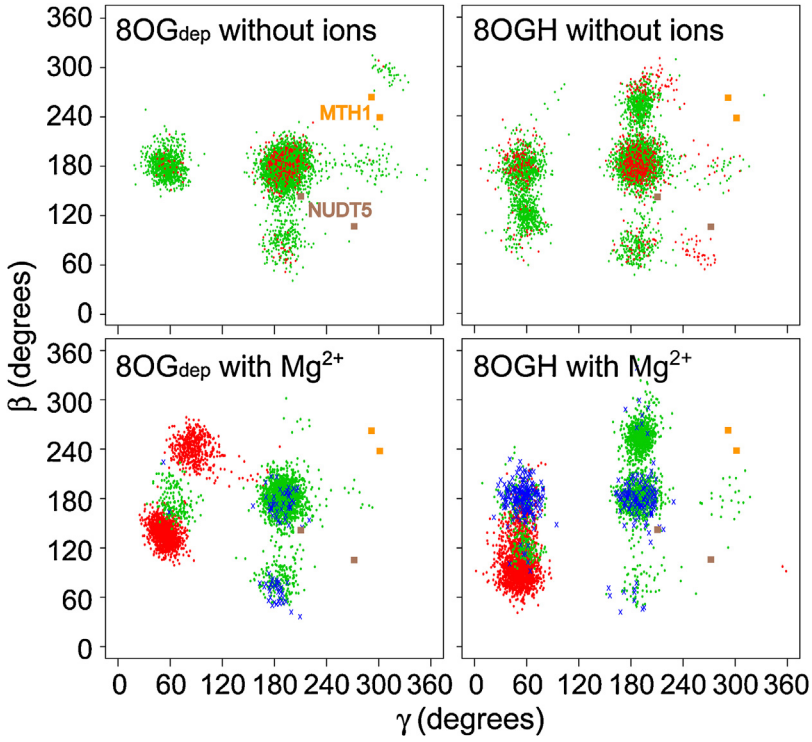

Fig. 4. Scatter plot of torsion angles (β, γ) of the sugar-phosphate backbone in the $8OG_{dep}$ and 8OGH systems using the χ_{std} parameter. In the systems without ions, green and red points indicate the *syn* and *anti* conformations, respectively. In the systems with Mg^{2+}, green, red, and blue points indicate the *syn* conformations, *anti* conformations obtained from MD simulations using the *anti* conformation as initial structures, and *anti* conformations obtained from MD simulations using the *syn* conformation as initial structures, respectively. β and γ angles of 8-oxo-dGMP or 8-oxo-dGDP in the crystal structures of MTH1 [5] and NUDT5 [6] are also shown. These figures are modified from Figs. S6 and S8 in Supporting information.

conformation. When the initial structure was the *syn* conformation, the proportion of the *syn* conformation was larger in the $dGMP_{dep}$ systems with Na^+ or Mg^{2+} than those without ions. In these systems, electrostatic interactions between the *syn* conformer of dGMP and metal ions were observed, as well as in the case of the MD simulations using the χ_{std} parameter (Fig. 2B and C). In dGMPH systems that used the *syn* conformation as the initial structure, the proportion of the *syn* conformation was larger than systems that used the *anti* conformation. Hydrogen bonding between the nitrogen atoms of guanine and the hydrogen atom of phosphate was observed in the *syn* conformation (Fig. 2B and C). The effect of protonation of phosphate, and the kinds of metal ions, on the *anti*/*syn* conformation of dGMP was observed more clearly in the χ_{mod} parameter than in the χ_{std} parameter.

When the *anti* conformation of 8-oxo-dGMP was the initial structure, the *anti* conformation was retained in both $8OG_{dep}$ and 8OGH systems without ions and with Na^+, as well as with Mg^{2+} (Fig. 5). This probably resulted from the higher energy barrier between the *anti* and *syn* conformations of mononucleotides in the

Table 3
Frequency of the *anti*-to-*syn* and *syn*-to-*anti* transitions, and maximum lifetime of the *anti*/*syn* conformations in MD simulations of dGMP using the χ_{mod} parameter.

Model	Initial structure	Frequency of transitions	Maximum lifetime (ps)[a]	
			Syn	*Anti*
$dGMP_{dep}$	*anti*	22	2	1620
	syn	12	223	2066
$dGMP_{dep} + Na^+$	*anti*	16	10	2653
	syn	86	1141	630
$dGMP_{dep} + Mg^{2+}$	*anti*	14	1	3146
	syn	152	≥5000[b]	12
dGMPH	*anti*	6	1	≥5000[b]
	syn	152	810	5
dGMPH + Na^+	*anti*	8	1	≥5000[b]
	syn	106	806	5
dGMPH + Mg^{2+}	*anti*	76	270	3123
	syn	63	1317	4255

[a] See footnotes of Table 1.
[b] The *anti* or *syn* conformationis retained during 5 ns in one of the two MD runs.

Table 4
Frequency of the *anti*-to-*syn* and *syn*-to-*anti* transitions, and maximum lifetime of the *anti*/*syn* conformations in MD simulations of 8-oxo-dGMP using the χ_{mod} force field.

Model	Initial structure	Frequency of transitions	Maximum lifetime (ps)[a]	
			Syn	*Anti*
$8OG_{dep}$	*anti*	41	511	2686
	syn	108	1460	3
$8OG_{dep} + Na^+$	*anti*	30	4	3416
	syn	96	1542	3
$8OG_{dep} + Mg^{2+}$	*anti*	0	0	≥5000[b]
	syn	112	1105	7
8OGH	*anti*	54	2044	962
	syn	86	1467	7
8OGH + Na^+	*anti*	94	513	1770
	syn	114	715	3
8OGH + Mg^{2+}	*anti*	0	0	≥5000[b]
	syn	154	811	195

[a] See footnotes of Table 1.
[b] The *anti* conformationis retained during 5 ns in both of the MD runs. The stability of the *anti* conformation is discussed in *Conformational sampling of mononucleotide using MD simulations* in Section 3.

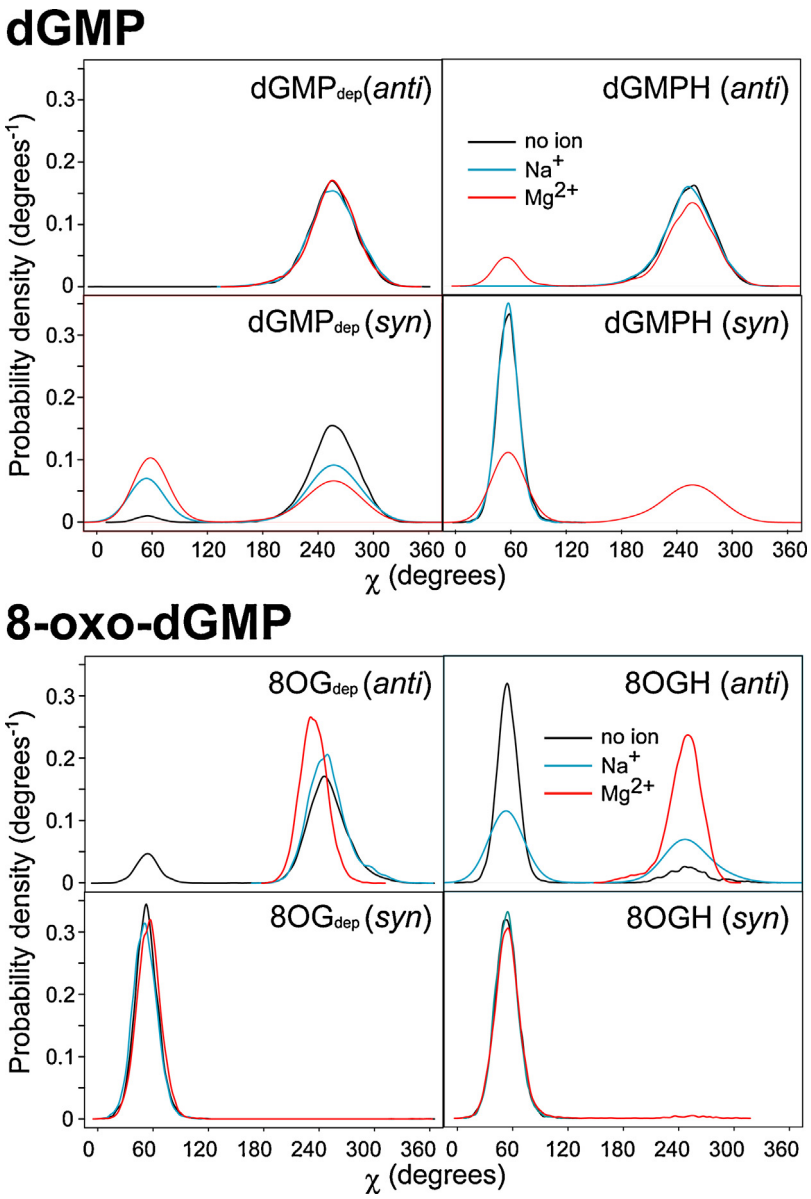

Fig. 5. Probability density of the χ angle of dGMP and 8-oxo-dGMP using the modified N-glycosidic bond parameter (χ_{mod}). Initial structures (*anti*/*syn*) are indicated in parentheses.

χ_{mod} parameter. In the 8OGH no-ion system, the mononucleotide adopted mainly the *syn* conformation because of the possible hydrogen bond between the nitrogen atoms of guanine and the hydrogen atom of phosphate (Fig. 2D). When the *anti* conformation was the initial structure, the proportion of the *anti* conformation was larger in the presence of Na^+ than without ions. The maximum lifetime of the *anti* conformation was longer in the 8OGH–Na^+ system than in the 8OGH no-ion system (Table 4). In the *anti* conformations observed in the 8OGH systems, Na^+ was located between the phosphate oxygen atom and the O8 atom in a manner similar to what was observed for Mg^{2+} (Fig. 3C). This suggested that metal ions other than Mg^{2+} can also retain the *anti* conformation of 8-oxo-dGMP.

3.4. Effect of ion size and charge on the conformations of 8-oxo-dGMP

The effects of Li^+ and Ca^{2+} were examined to elucidate whether ions other than Mg^{2+} can influence the conformations of 8-oxo-dGMP in a similar manner. Both Li^+ and Ca^{2+} differ from Mg^{2+} in terms of their ionic radii and charges. Table S1 summarizes the force field parameters of the metal ions used in this study. The ionic radius (corresponding to R^*) of Li^+ and the ionic radius of Ca^{2+} are similar with that of Mg^{2+}.

In terms of both χ_{std} and χ_{mod} parameters, 8-oxo-dGMP adopted both the *anti* and *syn* conformations in the presence of Li^+ and Ca^{2+} (Fig. 6). The observation that the proportion of the *anti* conformation was smaller in the presence of Li^+ and Ca^{2+} than with Mg^{2+} suggested that both ion size and charge can influence the proportion of the *syn*/*anti* conformations of 8-oxo-dGMP. The *syn*-to-*anti* transition was also observed in a series of MD simulations. In the 8OG$_{dep}$–Li^+ system, 8-oxo-dGMP shifted from the *syn* to *anti* conformation, and retained the stable state for a maximum of 393 ps (Table 5). The β and γ angles observed in the *anti* conformations with maximum lifetime were within the range of 130–200° and 150–210° (Fig. 7), which differed from the stable *anti* conformations observed in the 8OG$_{dep}$–Mg^{2+} and 8OGH–Mg^{2+} systems. In the *anti* conformations with maximum lifetime, Li^+ was often located

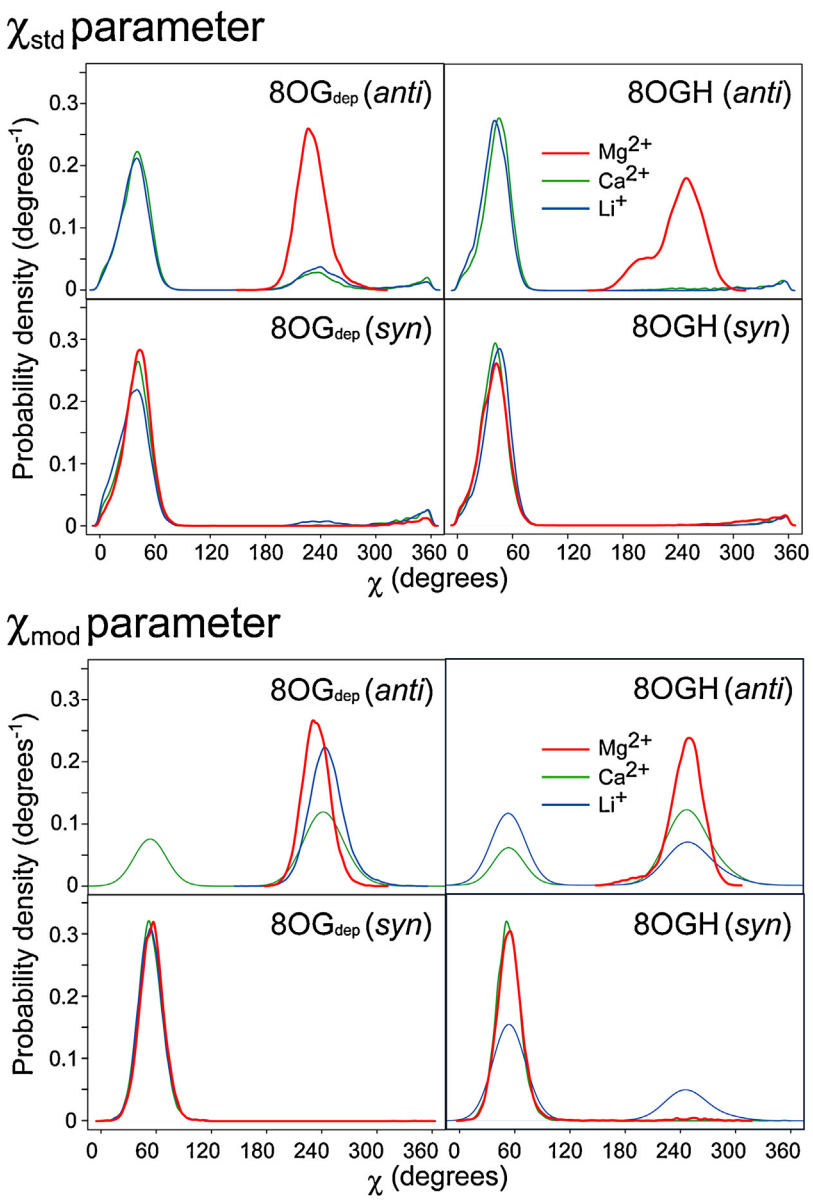

Fig. 6. Probability density of the χ angle of 8-oxo-dGMP in the $8OG_{dep}$ and 8OGH systems with Mg^{2+}, Li^{+} or Ca^{2+}. Initial structures (*anti*/*syn*) are indicated in parentheses.

between the phosphate oxygen atom and the O8 atom, similar to what was observed for Mg^{2+} (Fig. 3E). These results suggest that multiple types of stable *anti* conformers exist in 8-oxo-dGMP.

In this study, the force field parameter of Mg^{2+} was taken from the data by Åqvist [29]. This non-bonded model was adopted in early AMBER force fields. It is generally very difficult to model divalent ions for MD simulations because the non-bonded model of the interaction between the ions and their surrounding residues is oversimplified, and a single point poorly represents the charge distribution of most ions [42]. To overcome these problems, improvements in the force field parameter of Mg^{2+} have been devised [42–46]. For example, Allnér et al. [46] focused on the exchange rate between Mg^{2+} and water. They found from their MD simulations that the exchange rate between Mg^{2+} derived by Åqvist [29] and TIP3P water was slower than the experimental data. They developed a new set of Mg^{2+} parameters based on the Mg^{2+} – water exchange rate. In comparison with the non-bonded Mg^{2+} force field parameters recently developed [42–46], the ionic radius (R*) of Mg^{2+} derived by Allnér et al. [46] was close to that of Ca^{2+} derived by Åqvist (Table S1). Therefore, it is expected that the probability density profile of the χ angle in the $8OG_{dep}$ and 8OGH systems with Allnér's estimate for Mg^{2+}, using the *anti* conformation as the initial structure, may be close to that using Åqvist's estimate for Ca^{2+}. Although further improvements are needed to develop an accurate Mg^{2+} force field parameter, under the present MD simulations, the larger proportion of the *anti* conformation will be observed in the $8OG_{dep}$ and 8OGH systems with metal ions, and the types of the stable *anti* conformations might differ depending upon the properties of metal ions, such as ionic radius and charge.

3.5. Conformational sampling of mononucleotide using MD simulations

MD simulations are typically performed at laboratory temperatures and often require cost-prohibitive time scales to produce results that are consistent with those obtained by conformational sampling [47]. In the present 10-ns MD simulations, the conformational sampling of mononucleotides was sometimes influenced by the initial *anti* or *syn* conformations. In the χ_{mod} parameter, the probability density profiles were quite different between the initial

Table 5
Frequency of the *anti*-to-*syn* and *syn*-to-*anti* transitions, and maximum lifetime of the *anti*/*syn* conformations in MD simulations of 8-oxo-dGMP in the presence of Ca^{2+} or Li^{+}.

N-glycosidic torsion angle parameter	Model	Initial structure	Frequency of transitions	Maximum lifetime (ps)[a]	
				Syn	*Anti*
χ_{std}	$8OG_{dep}$ + Ca^{2+}	*anti*	66	1206	976
		syn	160	1287	71
	$8OG_{dep}$ + Li^{+}	*anti*	94	2717	892
		syn	114	1612	393
	8OGH + Ca^{2+}	*anti*	71	2395	119
		syn	56	1268	8
	8OGH + Li^{+}	*anti*	76	1599	54
		syn	52	1375	5
χ_{mod}	$8OG_{dep}$ + Ca^{2+}	*anti*	31	655	≥5000[b]
		syn	122	620	5
	$8OG_{dep}$ + Li^{+}	*anti*	16	2	≥5000[b]
		syn	112	916	7
	8OGH + Ca^{2+}	*anti*	45	532	2422
		syn	100	970	3
	8OGH + Li^{+}	*anti*	66	855	1532
		syn	87	467	104

[a] See footnotes of Table 1.
[b] The *anti* conformationis retained during 5 ns in one of the two MD runs.

anti and *syn* conformations (Fig. 5). In addition, when 8-oxo-dGMP was simulated in the presence of Mg^{2+} using the *anti* conformation as the initial structure, no *anti*-to-*syn* transition occurred (Tables 2 and 4). The transition did not occur even during the additional 95-ns MD simulations for each run (Fig. S11). Mg^{2+} was not moved away from the O8 atom of 8-oxo-dGMP (Fig. S12). The transitions were observed in the high-temperature (573 K) MD calculations. The simulations overcame the barriers between the *anti* and *syn* conformations in the $8OG_{dep}$ and 8OGH systems (starting conformation: *anti*) with Mg^{2+} (Fig. S13). The *anti*-to-*syn* transition occurred in either or both of the two MD runs of the $8OG_{dep}$ and 8OGH systems when Mg^{2+} was moved away from the O8 atom (Fig. S14). These findings indicate that the results of conformational sampling had not converged after two runs of the 5-ns MD simulations and that the probability density profiles of χ angle might be inaccurate. It is also possible that the force field parameter of Mg^{2+} derived by Åqvist [29] causes too strong an interaction between Mg^{2+} and the O8 atom of 8-oxo-dGMP. Enhanced sampling approaches, such as replica exchange MD [48], as well as improvements in the force field parameter of Mg^{2+} as discussed above, might be needed for converged sampling to obtain the accurate χ-angle probability density profiles of mononucleotides. However, a series of MD simulations of mononucleotides has clarified the effects of metal ions on the conformations of 8-oxo-dGMP.

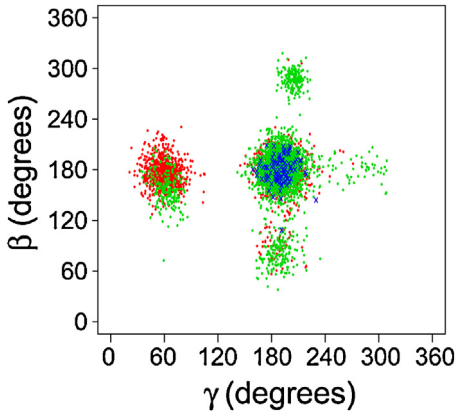

Fig. 7. Scatter plot of torsion angles (β, γ) of the sugar-phosphate backbone in the $8OG_{dep}$–Li^{+} system using the χ_{std} parameter. Green, red, and blue points indicate the *syn* conformations, *anti* conformations, and *anti* conformations with maximum lifetime obtained from MD simulations using the *syn* conformation as the initial structure, respectively. (For interpretation of the references to color in figure legend, the reader is referred to the web version of the article.)

4. Conclusions

A series of MD simulations of dGMP and 8-oxo-dGMP indicated that 8-oxo-dGMP can adopt both the *syn* and *anti* conformations. The proportion adopting the *anti* conformation increased in the presence of metal ions. When 8-oxo-dGMP adopted the *anti* conformation, metal ions were often located between the oxygen atom of phosphate and the O8 atom of 8-oxo-G. The types of stable *anti* conformations of 8-oxo-dGMP differed, depending on the ionic radii and charges of coexisting ions. This paper also described common issues associated with MD simulations, such as a lack of convergence, dependence on starting conformation, and dependability of force field parameters, particularly for ions. Further exploration of the dependence on χ dihedral parameters would be useful, not only for comparisons between parameters but also for gaining further insights into the conformations of mononucleotides. Nevertheless, there does seem to be a general trend in the MD simulations that the *anti* conformation of 8-oxo-dGMP is favored in the presence of metal ions. The MD results suggest the possibility that the 8-oxo-G deoxynucleotide adopts the *anti* conformation and binds to MTH1 or NUDT5. This study also suggested a role for metal ions other than as cofactors for the hydrolysis of di- and tri-phosphate forms of mononucleotides. Specifically, these ions can retain the *anti* conformation to promote the binding of 8-oxo-G deoxynucleotides to nucleotide-sanitizing enzymes. This study contributes to our understanding of the effects of metal ions and the protonation of mononucleotides on their conformations, and describes limitations and areas for improvement in order to gain further insights into conformations of mononucleotides through MD simulations.

Acknowledgement

This study was supported in part by Grants-in-Aid for Scientific Research from the Ministry of Education, Culture, Sports, Science and Technology of Japan (Grant no. 22500275).

Appendix A. Supplementary data

Supplementary data associated with this article can be found, in the online version, at http://dx.doi.org/10.1016/j.jmgm.2014.05.007.

References

[1] B. Van Loon, E. Markkanen, U. Hubscher, Oxygen as a friend and enemy: how to combat the mutational potential of 8-oxo-guanine, DNA Repair 9 (2010) 604–616.
[2] Y. Nakabeppu, K. Kajitani, K. Sakamoto, H. Yamaguchi, D. Tsuchimoto, MTH1, an oxidized purine nucleoside triphosphatase, prevents the cytotoxicity and neurotoxicity of oxidized purine nucleotides, DNA Repair 5 (2006) 761–772.
[3] H. Kamiya, M. Hori, T. Arimori, M. Sekiguchi, Y. Yamagata, H. Harashima, NUDT5 hydrolyzes oxidized deoxyribonucleoside diphosphates with broad substrate specificity, DNA Repair 8 (2009) 1250–1254.
[4] T. Nakamura, S. Meshitsuka, S. Kitagawa, N. Abe, J. Yamada, T. Ishino, H. Nakano, T. Tsuzuki, T. Doi, Y. Kobayashi, S. Fujii, M. Sekiguchi, Y. Yamagata, Structural and dynamic features of the MutT protein in the recognition of nucleotides with the mutagenic 8-oxoguanine base, J. Biol. Chem. 285 (2010) 444–452.
[5] L.M. Svensson, A.S. Jemth, M. Desroses, O. Loseva, T. Helleday, M. Hogbom, P. Stenmark, Crystal structure of human MTH1 and the 8-oxo-dGMP product complex, FEBS Lett. 585 (2011) 2617–2621.
[6] T. Arimori, H. Tamaoki, T. Nakamura, H. Kamiya, S. Ikemizu, Y. Takagi, T. Ishibashi, H. Harashima, M. Sekiguchi, Y. Yamagata, Diverse substrate recognition and hydrolysis mechanisms of human NUDT5, Nucl. Acids Res. 39 (2011) 8972–8983.
[7] S. Uesugi, M. Ikehara, Carbon-13 magnetic resonance spectra of 8-substituted purine nucleosides, characteristic shifts for the syn conformation, J. Am. Chem. Soc. 99 (1977) 3250–3253.
[8] J. Gidden, M.T. Bowers, Gas-phase conformations of deprotonated and protonated mononucleotides determined by ion mobility and theoretical modeling, J. Phys. Chem. B 107 (2003) 12829–12837.
[9] O.V. Shishkin, L. Gorb, O.A. Zhikol, J. Leszczynski, Conformational analysis of canonical 2-deoxyribonucleotides. 1. Pyrimidine nucleotides, J. Biomol. Struct. Dyn. 21 (2004) 537–554.
[10] O.V. Shishkin, L. Gorb, O.A. Zhikol, J. Leszczynski, Conformational analysis of canonical 2-deoxyribonucleotides. 2. Purine nucleotides, J. Biomol. Struct. Dyn. 22 (2004) 227–244.
[11] L. Gorb, O. Shishkin, J. Leszczynski, Charges of phosphate groups. A role in stabilization of 2′-deoxyribonucleotides. A DFT investigation, J. Biomol. Struct. Dyn. 22 (2005) 441–454.
[12] O.V. Shishkin, G.V. Palamarchuk, L. Gorb, J. Leszczynski, Intramolecular hydrogen bonds in canonical 2′-deoxyribonucleotides: an atoms in molecules study, J. Phys. Chem. B 110 (2006) 4413–4422.
[13] D. Liu, T. Wyttenbach, M.T. Bowers, Hydration of mononucleotides, J. Am. Chem. Soc. 128 (2006) 15155–15163.
[14] D. Kosenkov, L. Gorb, O.V. Shishkin, J. Sponer, J. Leszczynski, Tautomeric equilibrium, stability, and hydrogen bonding in 2′-deoxyguanosine monophosphate complexed with Mg^{2+}, J. Phys. Chem. B 112 (2008) 150–157.
[15] D.M. Close, K.T. Øhman, Ionization energies of the nucleotides, J. Phys. Chem. A 112 (2008) 11207–11212.
[16] D. Kosenkov, Y.A. Kholod, L. Gorb, O.V. Shishkin, G.M. Kuramshina, G.I. Dovbeshko, J. Leszczynski, Effect of a pH change on the conformational stability of the modified nucleotide queuosine monophosphate, J. Phys. Chem. A 113 (2009) 9386–9395.
[17] A.L. Millen, R.A. Manderville, S.D. Wetmore, Conformational flexibility of c8-phenoxyl-2′-deoxyguanosine nucleotide adducts, J. Phys. Chem. B 114 (2010) 4373–4382.
[18] G.V. Palamarchuk, O.V. Shishkin, L. Gorb, J. Leszczynski, Nucleic acid bases in anionic 2′-deoxyribonucleotides: a DFT/B3LYP study of structures, relative stability, and proton affinities, J. Phys. Chem. B 117 (2013) 2841–2849.
[19] F. Calvo, J. Douady, Stepwise hydration and evaporation of adenosine monophosphate nucleotide anions: a multiscale theoretical study, Phys. Chem. Chem. Phys. 12 (2010) 3404–3414.
[20] A. Grossfield, Recent progress in the study of G protein-coupled receptors with molecular dynamics computer simulations, Biochim. Biophys. Acta 1808 (2011) 1868–1878.
[21] R.M.C. Dawson, D.C. Elliot, W.H. Elliot, K.M. Jones, Data for Biochemical Research, 3rd ed., Clarendon Press, Oxford, 1986.
[22] AMBER11, University of California, San Francisco, 2010.
[23] J.M. Wang, P. Cieplak, P.A. Kollman, How well does a restrained electrostatic potential (RESP) model perform in calculating conformational energies of organic and biological molecules? J. Comput. Chem. 21 (2000) 1049–1074.
[24] H. Ode, Y. Matsuo, S. Neya, T. Hoshino, Force field parameters for rotation around chi torsion axis in nucleic acids, J. Comput. Chem. 29 (2008) 2531–2542.
[25] J.H. Miller, C.C. Fan-Chiang, T.P. Straatsma, M.A. Kennedy, 8-Oxoguanine enhances bending of DNA that favors binding to glycosylases, J. Am. Chem. Soc. 125 (2003) 6331–6336.
[26] N. Homeyer, A.H. Horn, H. Lanig, H. Sticht, AMBER force-field parameters for phosphorylated amino acids in different protonation states: phosphoserine, phosphothreonine, phosphotyrosine, and phosphohistidine, J. Mol. Model. 12 (2006) 281–289.
[27] Gaussian 03, Gaussian, Inc., Pittsburgh, 2003.
[28] W.L. Jorgensen, J. Chandrasekhar, J.D. Madura, R.W. Impey, M.L. Klein, Comparison of simple potential functions for simulating liquid water, J. Chem. Phys. 79 (1983) 926–935.
[29] J. Åqvist, Ion water interaction potentials derived from free-energy perturbation simulations, J. Phys. Chem. 94 (1990) 8021–8024.
[30] H.J.C. Berendsen, J.P.M. Postma, W.F. Van Gunsteren, A. DiNola, J.R. Haak, Molecular dynamics with coupling to an external bath, J. Chem. Phys. 81 (1984) 3684–3690.
[31] T. Darden, D. York, L. Pedersen, Particle mesh Ewald – an $N\log(N)$ method for Ewald sums in large systems, J. Chem. Phys. 98 (1993) 10089–10092.
[32] T. Darden, D. Pearlman, L.G. Pedersen, Ionic charging free energies: spherical versus periodic boundary conditions, J. Chem. Phys. 109 (1998) 10921–10935.
[33] W.F. Van Gunsteren, H.J.C. Berendsen, Algorithm for macromolecular dynamics and constraint dynamics, Mol. Phys. 34 (1977) 1311–1327.
[34] IUPAC-IUB Joint Commission on Biochemical Nomenclature, Abbreviations and symbols for the description of conformations of polynucleotide chains, Eur. J. Biochem. 131 (1983) 9–15.
[35] D.L. Nelson, M.M. Cox, Lehninger Principles of Biochemistry, 5th ed., W.H. Freeman and Company, New York, 2008.
[36] K. Fujikawa, H. Kamiya, H. Yakushiji, Y. Fujii, Y. Nakabeppu, H. Kasai, The oxidized forms of dATP are substrates for the human MutT homologue, the hMTH1 protein, J. Biol. Chem. 274 (1999) 18201–18205.
[37] K. Fujikawa, H. Kamiya, H. Yakushiji, Y. Nakabeppu, H. Kasai, Human MTH1 protein hydrolyzes the oxidized ribonucleotide, 2-hydroxy-ATP, Nucl. Acids Res. 29 (2001) 449–454.
[38] M. Mishima, Y. Sakai, N. Itoh, H. Kamiya, M. Furuichi, M. Takahashi, Y. Yamagata, S. Iwai, Y. Nakabeppu, M. Shirakawa, Structure of human MTH1, a Nudix family hydrolase that selectively degrades oxidized purine nucleoside triphosphates, J. Biol. Chem. 279 (2004) 33806–33815.
[39] T. Hollis, Y. Ichikawa, T. Ellenberger, DNA bending and a flip-out mechanism for base excision by the helix-hairpin-helix DNA glycosylase, *Escherichia coli* AlkA, EMBO J. 19 (2000) 758–766.
[40] I. Yildirim, H.A. Stern, S.D. Kennedy, J.D. Tubbs, D.H. Turner, Reparameterization of RNA chi torsion parameters for the AMBER force field and comparison to NMR spectra for cytidine and uridine, J. Chem. Theory Comput. 6 (2010) 1520–1531.
[41] M. Zgarbová, M. Otyepka, J. Šponer, A. Mládek, P. Banáš, T.E. Cheatham 3rd, P. Jurečka, Refinement of the Cornell et al. nucleic acids force field based on reference quantum chemical calculations of glycosidic torsion profiles, J. Chem. Theory Comput. 7 (2011) 2886–2902.
[42] F. Li, B.P. Roberts, D.K. Chakravorty, K.M. Merz Jr., Rational design of particle mesh Ewald compatible Lennard–Jones parameters for +2 metal cations in explicit solvent, J. Chem. Theory Comput. 9 (2013) 2733–2748.
[43] J. Florián, M.F. Goodman, A. Warshel, Computer simulation of the chemical catalysis of DNA polymerases: discriminating between alternative nucleotide insertion mechanisms for T7 DNA polymerase, J. Am. Chem. Soc. 125 (2003) 8163–8177.
[44] C.S. Babu, C. Lim, Empirical force fields for biologically active divalent metal cations in water, J. Phys. Chem. A 110 (2006) 691–699.
[45] P. Oelschlaeger, M. Klahn, W.A. Beard, S.H. Wilson, A. Warshel, Magnesium-cationic dummy atom molecules enhance representation of DNA polymerase beta in molecular dynamics simulations: improved accuracy in studies of structural features and mutational effects, J. Mol. Biol. 366 (2007) 687–701.
[46] O. Allnér, L. Nilsson, A. Villa, Magnesium ion-water coordination and exchange in biomolecular simulations, J. Chem. Theory Comput. 8 (2012) 1493–1502.
[47] J.L. Klepeis, K. Lindorff-Larsen, R.O. Dror, D.E. Shaw, Long-timescale molecular dynamics simulations of protein structure and function, Curr. Opin. Struct. Biol. 19 (2009) 120–127.
[48] Y. Sugita, Y. Okamoto, Replica-exchange molecular dynamics method for protein folding, Chem. Phys. Lett. 314 (1999) 141–151.
[49] W. Humphrey, A. Dalke, K.V.M.D. Schulten, Visual molecular dynamics, J. Mol. Graphics 14 (1996) 33–38.